Journal of Solid State Chemistry 183 (2010) 2352–2357

Contents lists available at ScienceDirect

Journal of Solid State Chemistry

journal homepage: www.elsevier.com/locate/jssc

Synthesis, crystal structure and thermal behavior of $Sr_3B_2SiO_8$ borosilicate

M.G. Krzhizhanovskaya [a,*], R.S. Bubnova [b], S.V. Krivovichev [a,b], O.L. Belousova [b], S.K. Filatov [a]

[a] Department of Crystallography, St. Petersburg State University, University Emb. 7/9, 199034 St. Petersburg, Russia
[b] Grebenshchikov Institute of Silicate Chemistry, Russian Academy of Sciences, Makarov Emb. 2, 199034 St. Petersburg, Russia

ARTICLE INFO

Article history:
Received 12 April 2010
Received in revised form
13 July 2010
Accepted 18 July 2010
Available online 24 July 2010

Keywords:
Sr borosilicate
Structure determination
Single crystal X-ray diffraction
Thermal expansion

ABSTRACT

Single crystals of $Sr_3B_2SiO_8$ were obtained by solid-state reaction of stoichiometric mixture at 1200 °C. The crystal structure of the compound has been solved by direct methods and refined to $R1=0.064$ ($wR=0.133$). It is orthorhombic, *Pnma*, $a=12.361(4)$, $b=3.927(1)$, $c=5.419(1)$ Å, $V=263.05(11)$ Å^3. The structure contains zigzag pseudo-chains running along the *b* axis and built up from corner sharing (Si,B)−O polyhedra. Boron and silicon are statistically distributed over one site with their coordination strongly disordered. Sr atoms are located between the chains providing three-dimensional linkage of the structure.

The formation of $Sr_3B_2SiO_8$ has been studied using annealing series in air at 900–1200 °C. According powder XRD, the probe contains pure $Sr_3B_2SiO_8$ over 1100 °C. The compound is not stable below 900 °C. In the pseudobinary $Sr_2B_2O_5$–$Sr_3B_2SiO_8$ system a new series of solid solutions $Sr_{3-x}B_2Si_{1-x}O_{8-3x}$ ($x=0$–0.9) have been crystallized from melt. The thermal behavior of $Sr_3B_2SiO_8$ was investigated using powder high-temperature X-ray diffraction (HTXRD) in the temperature range 20–900 °C. The anisotropic character of thermal expansion has been observed: $\alpha_a=-1.3$, $\alpha_b=23.5$, $\alpha_c=13.9$, and $\alpha_V=36.1\times10^{-6}$ °C^{-1} (25 °C); $\alpha_a=-1.3$, $\alpha_b=23.2$, $\alpha_c=5.2$, and $\alpha_V=27.1\times10^{-6}$ °C^{-1} (650 °C). Maximal thermal expansion of the structure along of the chain direction [0 1 0] is caused by the partial straightening of chain zigzag. Hinge mechanism of thermal expansion is discussed.

1. Introduction

Strontium borosilicate system has been used for a long time in ceramic industry for the fabrication of glaze glass coatings intended for the application on faience, porcelain, majolica, and other types of ceramics. Sr-containing glass is characterized by the high values of the refraction index, the volume resistivity, and the X-ray absorption coefficient. In the SrO–B_2O_3–SiO_2 system, glassforming and liquid immiscibility regions have been studied [1,2]. The data on different physical properties like viscosity [1,2], thermal expansion [3], density and micro-hardness [4] are reported. Glass structure in the system was discussed by Golubkov et al. [5]. Recent interest to the alkaline-earth borosilicate systems has been activated by their modern application for producing low-temperature cofired ceramic (LTCC) materials [6–9], widely used now for microwave, wireless, sensor, and other devices [http://www.ltcc.de/en/publications.php]. In [10], electronic properties and rare-earth ions photoluminescence behaviors in Sr-borosilicate, $SrB_2Si_2O_8$, were reported. Excellent photoluminescent properties were briefly noted for Eu^{2+}-activated $SrB_2Si_2O_8$ in [11].

Crystallographic data on crystalline Sr borosilicates as well as for the other alkaline-earth borosilicates are very limited. First the subsolidus relations in SrO–B_2O_3–SiO_2 system were investigated by solid-state reaction techniques and powder X-ray diffraction (XRD) methods in [12]. A stable ternary $Sr_3B_2SiO_8$ compound, and a metastable ternary compound with a probable composition $SrB_2Si_2O_8$ were reported and unindexed XRD data were presented for both of them (PDF ## 32-1224 and 31-1347). Twenty years later, the structure of high pressure synthetic compound $SrB_2Si_2O_8$ was solved in the orthorhombic space group *Pnam* [13]. The structure was found to be isotypic with $CaB_2Si_2O_8$ danburite structure, first reported in 1931 [14] and later refined by many authors [15–17 and others] and even at high temperatures [18]. The structure of $SrB_2Si_2O_8$ represents three-dimensional framework built up from ordered BO_4 and SiO_4 tetrahedra forming 4- and 8-membered rings. Not long ago, two naturally occurring Sr- and Ba-dominant analogues of danburite (pekovite, $SrB_2Si_2O_8$, and maleevite, $BaB_2Si_2O_8$) were found in alkaline massifs and structurally characterized by Pautov et al. [19].

Present work is devoted to the study of crystal structure and thermal behavior of stoichiometrically different Sr borosilicate—$Sr_3B_2SiO_8$, which was first mentioned in [12] and shortly noted by us in [20], but never structurally characterized.

2. Experimental

2.1. Synthesis and heat treatment of samples

$Sr_3B_2SiO_8$ powder and single crystals were prepared by solid-state reaction from SiO_2, H_3BO_3, and preliminary calcinated $SrCO_3$.

* Corresponding author. Fax: +7 812 3289775.
E-mail address: krzhizhanovskaya@mail.ru (M.G. Krzhizhanovskaya).

0022-4596/$ - see front matter © 2010 Elsevier Inc. All rights reserved.
doi:10.1016/j.jssc.2010.07.029

Initial charge was heat-treated in a platinum crucible in a furnace in the temperature range 900–1200 °C. Heating and cooling rate for sample preparation is about 5 and 1 K/min, respectively. Powder diffraction patterns of heat-treated materials were obtained with a Stoe Stadi P diffractometer (CuKα_1 radiation; λ=1.5406 Å, 40 kV/35 mA, PSD detector, curved Ge-monochromator). Small single crystals were obtained both in probes heat-treated at 1100 and 1200 °C. The temperature of 1200 °C is a bit higher than 1180 °C, noted in [21] as a melting point for the compound. In this case, the probe was probably partially melted. In the probe heat-treated at 1100/3 h and 1200 °C for 3 h small plated colorless crystals of $Sr_3B_2SiO_8$ were observed with the use of an optical microscope. These crystals have been used then for the single crystal diffraction study.

Solid solutions of $Sr_{3-x}B_2Si_{1-x}O_{8-3x}$ (x=0.37, 0.63, 0.84) were prepared in the pseudobinary $Sr_2B_2O_5$–$Sr_3B_2SiO_8$ system by crystallization of a melt. Before melting, the samples were heat-treated in the range 900–1200 °C.

2.2. Crystal structure study

A set of colorless crystals selected for data collection was examined under an optical microscope and mounted on glass fibers. Single crystal X-ray experiments were performed using a STOE Imaging Plate Diffraction System (IPDS) (MoKα radiation; λ=0.71073 Å, 50 kV/40 mA, frame widths of 1° in ω). Most of the checked crystals were found to be defective. First the unit-cell parameters and orthorhombic symmetry for $Sr_3B_2SiO_8$ were shortly noted by us in the abstract of an IUCr Congress [20]. The obtained R-factor ($R1\sim0.10$) did not allow us to present the crystal structure data at that time. In the present study, a small piece was found, which appeared to be suitable for structure determination. Since the standard tests did not clearly indicate the existence of centre of symmetry, the structure was refined in both non-centrosymmetric ($Pn2_1a$) and centrosymmetric ($Pnma$) space groups. It should be noted that refinement in the centrosymmetric group $Pnma$ yielded a slightly lower reliability factor (wR=0.133) in comparison to that assuming $Pn2_1a$ (wR=0.145); meanwhile $R1$-factors were practically the same. Atomic coordinates of the structure and the calculated bond lengths were similar for both of these groups; although the values of estimated standard deviations were substantially lower for the centrosymmetric case. Thus, the structure is reported here in the centrosymmetric space group $Pnma$. The unit-cell dimensions were refined by least-squares method (Table 1). The unit-cell parameters reported in [20] slightly differ from the data presented here that is caused by the tendency of the $Sr_3B_2SiO_8$ structure to a wide range of B–Si substitution (see below Section 3.2).

The raw intensities were corrected for Lorentz and polarization effects. The absorption correction was applied taking into account the form of the crystal with the use of X-Area (Stoe) program. The structure was solved by direct methods and refined with SHELXL-97 program package [22]. The final model included anisotropic displacement parameters for Sr only. Attempts to refine anisotropic parameters of O and (B,Si) positions resulted in physically unrealistic values. Technical details of the data acquisition as well as some refinement results for the title compound are summarized in Table 1. The atomic coordinates, displacement parameters, and site occupancies are given in Table 2. The refinement of occupancies of Sr and B,Si sites did not reveal any non-stoichiometry. In final refinement, the occupancies were fixed in order to fulfill electroneutrality requirements; direct refinement would result in some discrepancies from the required stoichiometry. In general, standard deviation errors for occupancies may be estimated as 0.04.

2.3. High-temperature X-ray powder diffraction study

Thermal expansion of an $Sr_3B_2SiO_8$ was studied in air by means of high-temperature X-ray powder diffraction data collected using a Stoe Stadi P X-ray diffractometer (CuKα radiation) with a high-temperature camera (Buehler GMbh). The sample was prepared from the heptane's suspension on a Pt–Rh plate. The temperature steps were 25 °C, average heating rate was about 1–2 °C/min in the range 20–900 °C. Unit-cell parameters of the compound at

Table 1
Crystallographic data and refinement parameters for $Sr_3B_2SiO_8$.

Crystal size (mm^3)	$0.03\times0.07\times0.08$
Formula weight (g/mol)	190.52
Structural formula	$SrB_{0.67}Si_{0.33}O_{2.67}$
Space group	$Pnma$
Z	4
a (Å)	12.361(4)
b (Å)	3.927(1)
c (Å)	5.419(1)
V ($Å^3$)	263.05(11)
μ (mm^{-1})	20.367
D_{calc} (g/cm^3)	3.705
Diffractometer	STOE IPDS II
Radiation wavelength (Å)	0.71073 (MoKα)
θ-range (°)	3.30–29.13
Total Ref	2046
Unique Ref	400
Unique $\lvert Fo\rvert \geq 4\sigma_F$	369
R_{int}	0.086
R_s	0.045
R (2064 Ref)	0.070
R ($\lvert Fo\rvert \geq 4\sigma_F$)	0.064
wR (2064 Ref)	0.133
wR ($\lvert Fo\rvert \geq 4\sigma_F$)	0.129
S	1.179

Table 2
Atomic coordinates and displacement parameters ($Å^2$) for $Sr_3B_2SiO_8$.

Atom	Wyck	x	y	z	U iso/eq[a]	Occupancy[b]
Sr	4c	0.1463(1)	0.75	0.9054(2)	0.0393(6)	1
B	4c	0.4170(6)	0.75	0.9336(15)	0.040(2)	0.67
Si	4c	0.4170(6)	0.75	0.9336(15)	0.040(2)	0.33
O(1)	4c	0.4240(16)	0.75	0.674(3)	0.041(4)	0.58
O(2)	8d	0.513(2)	0.914(7)	0.933(5)	0.049(7)	0.25
O(3)	4c	0.342(2)	0.75	0.115(4)	0.038(5)	0.60
O(4)	4c	0.3668(15)	0.75	0.675(3)	0.034(4)	0.50
O(5)	4c	0.317(2)	0.75	0.088(5)	0.040(7)	0.48

[a] anisotropic displacement parameters for an Sr atom: Sr 0.0734(10) 0.0212(6) 0.0232(6) 0.000 –0.0165(6) 0.000.

[b] In final refinement, occupancies were fixed in order to fulfill electroneutrality requirements; standard deviation errors may be estimated as 0.04.

Table 3
Selected bond lengths in the $Sr_3B_2SiO_8$ structure.

Bond	Distance (Å)	Occupancy of O ligand	Bond	Distance (Å)
Sr–O(5)	2.33(3)	0.48	T–O(3)	1.36(2)
Sr–O(4)×2	2.45(1)	0.50×2	T–O(2)×2	1.35(3)
Sr–O(3)×2	2.52(1)	0.60×2	T–O(1)	1.41(2)
Sr–O(2)×2	2.55(3)	0.25×2	T–O(5)	1.50(2)
Sr–O(1)×2	2.59(1)	0.58×2	T–O(4)	1.53(2)
Sr–O(5)×2	2.65(2)	0.48×2	T–O(2)×2	1.73(3)
Sr–O(3)	2.67(2)	0.60		
Sr–O(1)	2.78(2)	0.58		
		Σ 6.48		

different temperatures were refined by least-square methods. Main coefficients of the thermal expansion tensor were determined using polynomial approximation of temperature dependencies for the unit-cell parameters in the range 20–900 °C by DTC and DTP programs [23].

3. Results

3.1. Crystal structure of $Sr_3B_2SiO_8$

Selected bond lengths in the structure of $Sr_3B_2SiO_8$ are listed in Table 3. General motif of the structure is a pseudo-chain consisting of corner sharing TO_x polyhedra (T=B, Si; x=3–4) (Fig. 1). The statistical distribution of boron and silicon over one crystallographic site was successfully used for structure determination; meanwhile, the refinement evidenced that the oxygen coordination for (Si,B) site is highly disordered. As can be seen from Fig. 1c, there are eight possible sites for the O atoms visually constructing tetrahedra with splitted positions of each oxygen atoms. "Pseudo tetrahedral" coordination is strongly distorted; the T–O distances have a large spread of values especially for the atoms with small occupancies (see Fig. 1c and Table 2 atoms O(2) and O(3)). It seems that up to now the most distorted BO_4 tetrahedra were found in the structure of cubic β-$Mg_3ClB_3O_{13}$ boracite with three equal distances 1.437 and one elongated bond 1.693 Å in tetrahedra [24]. Although the average distances in tetrahedra should be around 1.48 Å for BO_4 [25,26] and 1.62 Å for SiO_4 [27], wide variations of individual interatomic distances in tetrahedra are described in [27] for silicates and

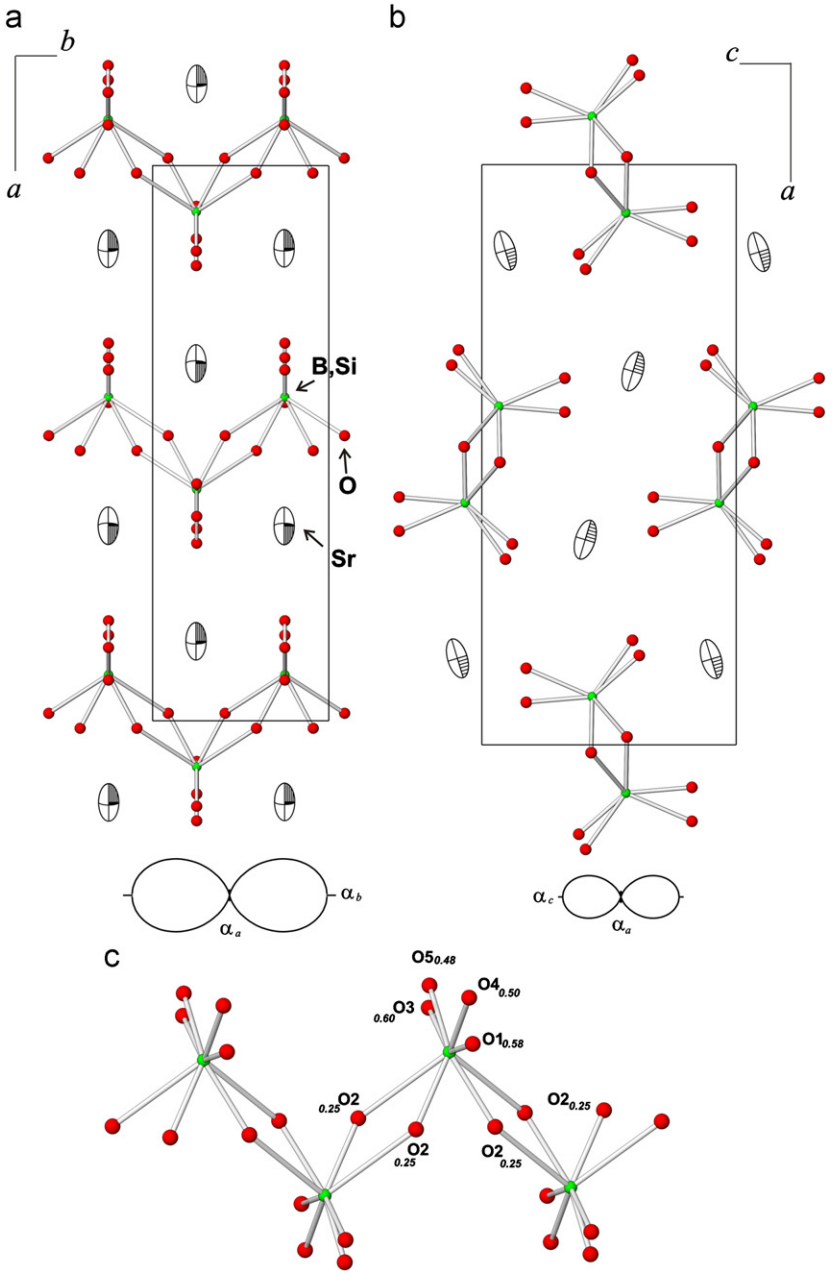

Fig. 1. Crystal structure of $Sr_3B_2SiO_8$ and pole figure of its thermal expansion coefficients: *ab* (a) and *ac* (b) projections; fragment of zigzag pseudochain (c). Italic numbers near the atom labels are devoted to the site occupancies.

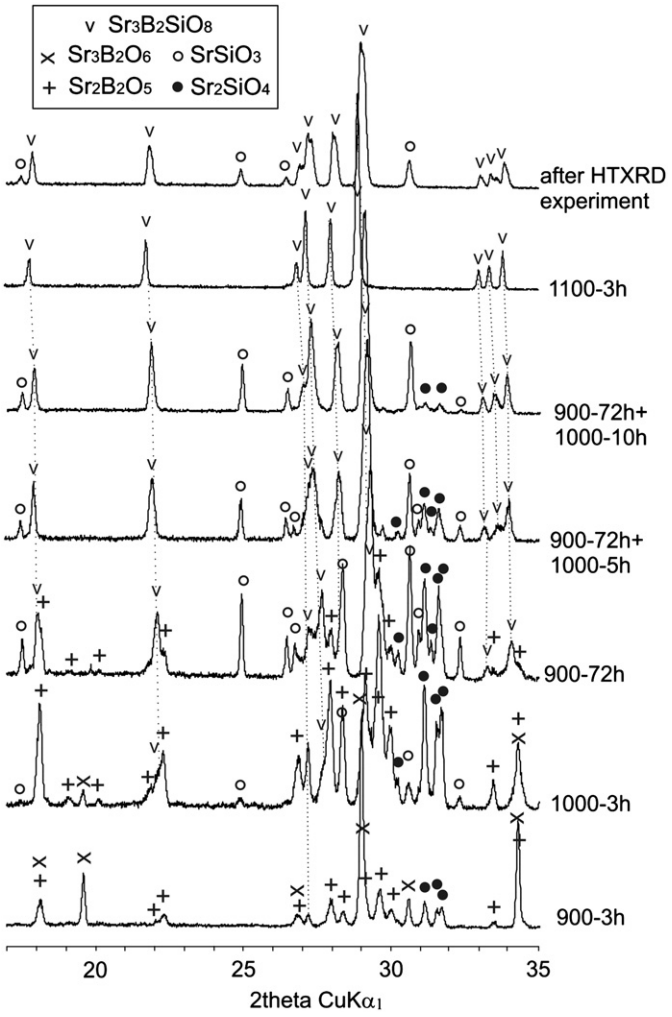

Fig. 2. Formation of $Sr_3B_2SiO_8$ during solid-state reaction.

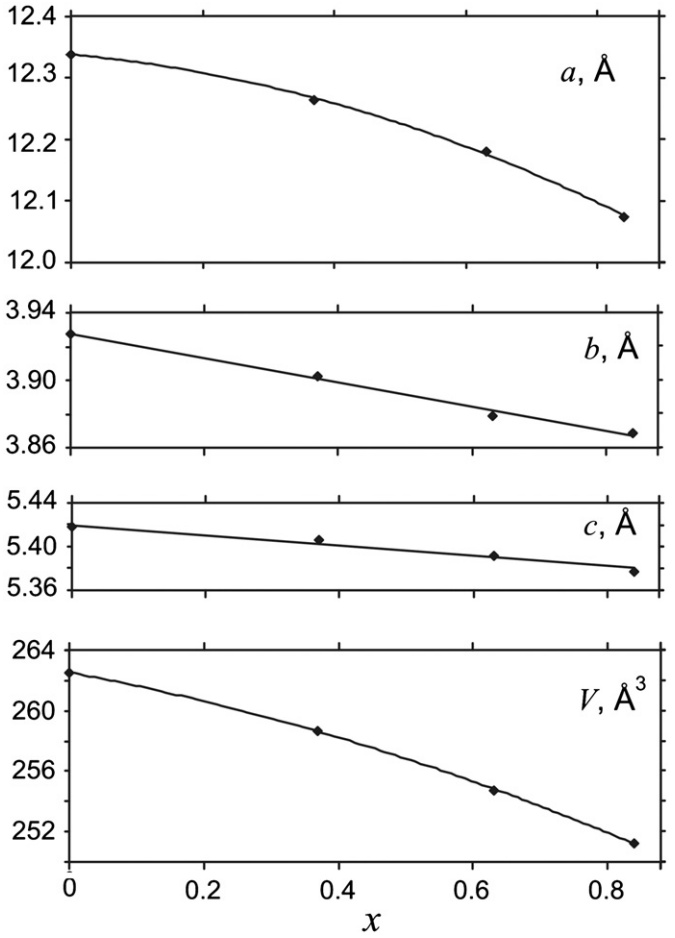

Fig. 3. Unit-cell parameters of $Sr_{3-x}B_2Si_{1-x}O_{8-3x}$ solid solutions in dependence of chemical composition.

[25,28,29] for borates. Chains comprise a zigzag along the [0 1 0] direction. Sr atoms occupying the space between the chains have irregular coordination (Table 3). Approximately 6.5 oxygen atoms coordinate Sr atom with the bond lengths below 3 Å (2.33–2.78 Å). Similar coordination was reported for the nearest neighbor compound $Sr_2B_2O_5$ [30]: $Sr(1)O_7$ (2.42–2.74 Å) and $Sr(2)O_6$ (2.46–2.55 Å).

Obviously, the wide variations of *T*–O distances in $Sr_3B_2SiO_8$ could be explained by the observed disorder of boron and silicon coordination. The chemical formula of the chain can be written as $[B_2SiO_8]^{6-}$, which implies that, within the chain, there are three polyhedra, SiO_4, BO_4, and BO_3, condensed through the corners: $[BO_3BO_2SiO_3]^{6-}$. Thus, generally Si atoms always have a tetrahedral coordination, whereas boron atoms are distributed in equal proportion between tetrahedra and triangles.

3.2. Formation of $Sr_3B_2SiO_8$ and $Sr_{3-x}B_2Si_{1-x}O_{8-3x}$ solid solutions

According to Baylor and Brown [12], the title compound was formed by reacting $SrSiO_3$ and $Sr_2B_2O_5$ or Sr_2SiO_4 and SrB_2O_4 at 1100 °C for 10 days. However, the authors did not obtain a pure phase: the XRD pattern presented in the PDF file (PDF 32-1224) and in [12] contained main reflections of $Sr_3B_2O_6$ (*d*, Å/*I*,%: 3.55/3; 3.21/5; 2.91/>2; 2.885/25; 2.876/13) along with maxima of $Sr_3B_2SiO_8$. In this work, polycrystalline $Sr_3B_2SiO_8$ has been synthesized by solid-state reaction, as described in Section 2.1. The XRD patterns after the annealing stages are presented in Fig. 2. During the solid-state reaction, borate phases crystallize first as intermediate products. In particular, $Sr_3B_2O_6$ crystallizes with an admixture of $Sr_2B_2O_5$ and traces of Sr_2SiO_4 by keeping the starting mixture at 900 °C for 3 h (Fig. 2, bottom XRD pattern). After the following short treatment at 1000 °C for 3 h, the intensity of $Sr_3B_2O_6$ peaks decreases; weak traces of $Sr_3B_2SiO_8$ appeared. Long-term treatment of an initial mixture performed at 900 °C for 3 days (72 h) showed that the title compound starts to form at this temperature. The broadened maxima of this phase could be identified (Fig. 2), although they are remarkably shifted in 2θ from the theoretical positions calculated from structural data, which possibly indicates a non-stoichiometric nature of the phase. The approximate unit-cell dimensions calculated for this phase treated at lower temperatures (900/72 h+1000/5 h: $a=12.221(9)$, $b=3.887(4)$, $c=5.395(3)$ Å, $V=256.3(3)$ Å^3; 900/72 h+1000/10 h: $a=12.288(4)$, $b=3.903(2)$, $c=5.404(2)$ Å, $V=259.2(1)$ Å^3) are less than that of after the treatment at 1100 °C. It is very likely an evidence that the phase forms by the step-by-step process. The decrease of the cell parameters indicates that SiO_2-poor phase crystallizes first, and then gradually transforms to $Sr_3B_2SiO_8$. Over 1100 °C, the probe contains pure $Sr_3B_2SiO_8$; the unit-cell parameters do not change after the treatment at 1200 °C. Below 900 °C, the compound is unstable (see Section 3.3).

The conclusions mentioned above are confirmed by occurrence of $Sr_{3-x}B_2Si_{1-x}O_{8-3x}$ solid solutions in the pseudobinary

$Sr_2B_2O_5$–$Sr_3B_2SiO_8$ system. The solid solutions are prepared by crystallization from melt and their studies are in progress. The dependence of unit-cell parameters versus chemical composition is shown in Fig. 3. It can be seen that parameters decrease along with decrease of the SiO_2 content: e.g., unit-cell dimensions for $Sr_{2.16}B_2Si_{0.16}O_{5.48}$ ($x=0.84$) are: $a=12.076(1)$, $b=3.8689(8)$, $c=5.3774(7)$ Å, $V=251.23(3)$ Å^3. From the unit-cell parameters dependence (Fig. 3), we could estimate approximately chemical composition of the nonstoichiometric phase crystallized after annealing at lower temperatures (900/72 h+1000/5 h: it is close to that with $x\approx 0.5\div 0.6$; 900/72 h+1000/10 h: and it is close to that with $x\approx 0.3\div 0.4$).

Crystal structures of $Sr_2B_2O_5$ and $Sr_3B_2SiO_8$ are similar (Fig. 4). Actually, $Sr_2B_2O_5$ is a nearest neighbor of $Sr_3B_2SiO_8$ in the phase diagram of the SrO–B_2O_3–SiO_2 system [12]. $Sr_2B_2O_5$ [30] crystallizes in the monoclinic space group $P2_1/c$ ($a=7.719(4)$, $b=5.341(1)$, $c=11.873(2)$ Å, $\beta=92.71(2)^\circ$, $V=488.9(3)$ Å^3) and is based upon isolated B_2O_5 groups of two corner sharing triangles (Fig. 4, *left*). When compared to $Sr_3B_2SiO_8$, $Sr_2B_2O_5$ has the a parameter increasing twice, whereas other parameters are practically the same. Substitution of B by Si is accompanied by an intercalation of additional oxygen atoms to form disordered tetrahedra in the $Sr_{3-x}B_2Si_{1-x}O_{8-3x}$ solid solutions. It could be assumed that isolated B_2O_5 groups in $Sr_2B_2O_5$ (Fig. 4, *left*) are transformed (polymerized) to pseudo-tetrahedral chains in our structure, due to the incorporation of silicon. This results in the transformation of isolated B_2O_5 groups via condensation into chains of $(B,Si)O_4$ tetrahedra, as shown in Fig. 4. The $Sr_{3-x}B_2Si_{1-x}O_{8-3x}$ ($x\approx 0\div 0.9$) solid solutions are extended almost to $Sr_2B_2O_5$. Immiscibility is caused by the difference in symmetry of $Sr_2B_2O_5$ and $Sr_3B_2SiO_8$ and nonexistence of silicon atoms in triangles.

3.3. Thermal behavior of $Sr_3B_2SiO_8$ from high-temperature X-ray diffraction

Thermal behavior of $Sr_3B_2SiO_8$ was investigated by *in situ* X-ray high-temperature powder diffraction in the temperature range 20–900 °C. For the experiment, the samples containing pure $Sr_3B_2SiO_8$ prepared by solid-state reaction at 1100 and 1200 °C have been used. The thermal changes in both samples were the same. The evolution of XRD patterns at different temperatures is presented in Fig. 5 for the $Sr_3B_2SiO_8$ sample prepared at 1200 °C. In the course of study, several reflections of $SrSiO_3$ (marked by arrows in Fig. 5) appeared at 770 °C that indicates the start of the $Sr_3B_2SiO_8$ decomposition. As it is shown in Section 3.2, the $Sr_3B_2SiO_8$ compound starts to form at 900 °C; below this temperature, the compound is not stable. During HTXRD experiment, the compound decomposes above 770 °C forming SiO_2-poor nonstoichiometric phase and $SrSiO_3$ (Figs. 5 and 2—the top XRD pattern). Hence, single-phase $Sr_3B_2SiO_8$ exists within the temperature range $20\div 770$ °C, and above 770 °C the biphasic region is observed.

The unit-cell parameters were calculated in the temperature range 20–900 °C (Fig. 6). The temperature dependences of orthorhombic unit-cell parameters demonstrate a flexion at about 650–700 °C caused obviously by the compositional changes, although $SrSiO_3$ reflections in the XRD pattern were observed at higher temperature (Fig. 5). For further determination of thermal expansion coefficients of $Sr_3B_2SiO_8$, the single-phase temperature region (20–650 °C) has been used only. The temperature dependencies show a distinctive anisotropy of expansion along crystallographic directions with maximal expansion along the minimal crystallographic b parameter (Fig. 6). The temperature dependences of the a and b parameters are approximated linearly, while that of the c parameter using quadratic equation

$$a = 12.3325 - 15.8\times 10^{-6} t$$
$$b = 3.9227 + 92.6\times 10^{-6} t$$
$$c = 5.4101 + 75.0\times 10^{-6} t - 4\times 10^{-8} t^2$$

Thermal expansion coefficients are as follows: $\alpha_a = -1.3$, $\alpha_b=23.5$, $\alpha_c=13.9$, and $\alpha_V=36.1\times 10^{-6}$ °C^{-1} at 25 °C; $\alpha_a = -1.3$, $\alpha_b=23.2$, $\alpha_c=5.2$ and $\alpha_V=27.1\times 10^{-6}$ °C^{-1} at 600 °C. Two projections of the $Sr_3B_2SiO_8$ structure are presented in Fig. 1 compared with the projections of pole figure of thermal expansion coefficients. Anisotropy of thermal expansion is not typical for chain structures: maximal expansion is observed along the tetrahedral chain, due to partial straightening of the chain zigzag. The chain expansion is governed by the so-called hinge mechanism [29,31]—if the structure expands along the chain axis [0 1 0] ($\alpha_b=23.5\times 10^{-6}$ °C^{-1}), it has to contract in the perpendicular plane ac ($\alpha_a = -1.3\times 10^{-6}$ °C^{-1}). The maximal expansion along the chain direction could be explained by

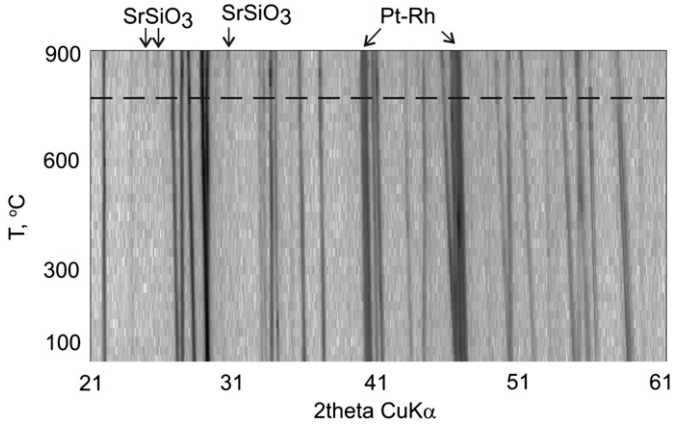

Fig. 5. HTXRD patterns of $Sr_3B_2SiO_8$. $SrSiO_3$ and Pt–Rh peaks are marked by arrows. The dashed line shows the temperature of $SrSiO_3$ reflections appearing.

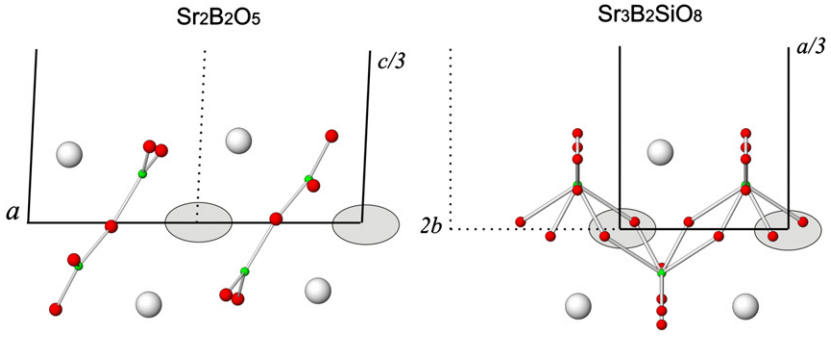

Fig. 4. The comparison of $Sr_2B_2O_5$ and $Sr_3B_2SiO_8$ structures.

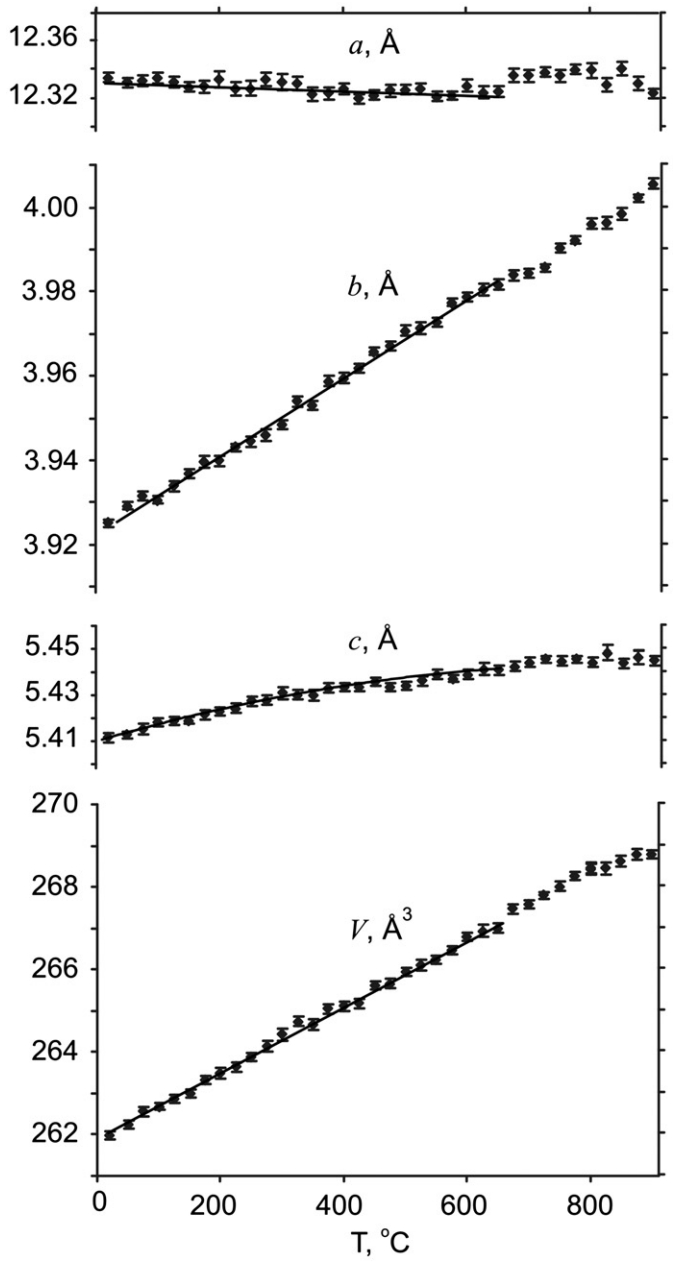

Fig. 6. Temperature dependence of orthorhombic cell parameters of $Sr_3B_2SiO_8$.

relatively weak bonding caused by incomplete occupancies of bridging oxygen sites O(2). Another reason for straightening of the chain zigzag could be strong vibrations of Sr atoms in the *a* direction (Fig. 1). The volumetric expansion coefficient is practically the same as an average one for borosilicates ($36\times10^{-6}\,^{\circ}C^{-1}$) and slightly higher than that of silicates ($23\times10^{-6}\,^{\circ}C^{-1}$) [29].

4. Conclusion

The new crystal structure of $Sr_3B_2SiO_8$ borosilicate was solved on a single crystal prepared from stoichiometric mixture by solid-state reaction at 1200 °C. Crystal structure presents a new structure type and contains a new borosilicate pseudo-chain anion $[B_2SiO_8]^{6-}$. The structure is significantly disordered. The chemical formula of the chain implies that, within the chain, there are three polyhedra, SiO_4, BO_4, and BO_3, condensed through the corners: $[BO_3BO_2SiO_3]^{6-}$. Thus, generally Si atoms always have a tetrahedral coordination, whereas boron atoms are distributed in equal proportion between tetrahedra and triangles.

The compound starts to form at 900 °C by solid-state reactions: first an intermediate nonstoichiometric SiO_2-poor phase $Sr_{3-x}B_2Si_{1-x}O_{8-3x}$ crystallizes. Stoichiometric $Sr_3B_2SiO_8$ compound is obtained at 1100–1200 °C. Below 900 °C, $Sr_3B_2SiO_8$ is not stable in accord to HTXRD data. The $Sr_{3-x}B_2Si_{1-x}O_{8-3x}$ ($x\approx0\div0.9$) solid solutions were prepared by crystallization of a melt.

Maximal thermal expansion of the structure along of the [0 1 0] is caused by the partial straightening of chain zigzag. Anisotropy of thermal expansion could be explained by strong vibrations of strontium atoms located between the zigzag chains.

Acknowledgment

The studies are supported by Russian Foundation for Basic Research (Project # 10-03-00732).

Appendix A. Supplementary material

Supplementary data associated with this article can be found in the online version at doi:10.1016/j.jssc.2010.07.029.

References

[1] R. Baylor, J.J. Brown, J. Amer., Ceram. Soc. 59 (1976) 131–136.
[2] S.V. Stolyar, N.G. Tyurnina, Z.G. Tyurnina, L.A. Doronina, Glass Phys. Chem. 34 (2008) 509–511.
[3] S.V. Stolyar, N.G. Tyurnina, Glass Phys. Chem. 35 (2009) 149–152.
[4] N.G. Turnina, Z.G. Turnina, S.I. Sviridov, Glass Phys. Chem. 35 (2009) 153–157.
[5] V.V. Golubkov, N.G. Turnina, Z.G. Turnina, V.L. Stolyarova, Glass Phys. Chem. 35 (2009) 455–462.
[6] R.R. Tummala, J. Am. Ceram. Soc. 74 (1991) 895–908.
[7] J.-H. Jean, Yu-C. Fang, S.X. Dai, D.L. Wilcox, J. Mater. Res. 17 (2002) 1772–1778.
[8] Y. Liu, Y. Wang, J. Ma, Eng. Mater. 336–338 (2007) 783–785.
[9] C.-C. Chiang, S.-F. Wang, Y.-R. Wang, W.-C.J. Wei, Ceram. Int. 34 (2008) 599–604.
[10] Y. Wang, Z. Zhang, J. Zhang, Y. Lu, J. Solid State Chem. 182 (2009) 813–820.
[11] J.M.P.J Verstegen, J.W. Ter Vrugt, W.L. Wanmaker, J. Inorg. Nucl. Chem. 34 (1972) 3588–3589.
[12] R. Baylor, J.J. Brown, J. Am. Ceram. Soc. 59 (1976) 21–23.
[13] T. Berger, K.-J. Range, Z. Naturforsch. B: Chem. Sci. 51 (1996) 172–174.
[14] C. Dunbar, F. Machatschki, Z. Kristallogr. 76 (1931) 133–146.
[15] G. Johansson, Acta Crystallogr. 12 (1959) 522–525.
[16] M.W. Phillips, G.V. Gibbs, P.H. Ribbe, Am. Mineral. 59 (1974) 79–85.
[17] J.W. Downs, R.J. Swopel, J. Phys. Chem. 96 (1992) 4834–4840.
[18] K. Sugiyama, Y. Takéuchi, Z. Kristallogr. 173 (1985) 293–304.
[19] L.A. Pautov, A.A. Agakhanov, E.V. Sokolova, F.C. Hawthorne, *Can. Mineral.* 42 (2004) 107–119.
[20] M.G. Krzhizhanovskaya, R.S. Bubnova, S.K. Filatov, Acta Crystallogr. A64 (2008) C504.
[21] N.G. Turnina, O.L. Belousova, A.I. Domansky, L.A. Doronina, V.L. Ugolkov, *Glass Phys. Chem.* 36 (2010) 294–304.
[22] G.M. Sheldrick, SHELXL-97, Program for the Refinement of Crystal Structures, Universität Göttingen, Germany, 1997.
[23] R.V. Belousov, S.K. Filatov, Glass Phys. Chem. 33 (2007) 271–275.
[24] S. Sueno, J.R. Clark, J.J. Papike, J.A. Konnert, Am. Mineral. 58 (1973) 691–697.
[25] F.C. Hawthorne, P.C. Burns, J.D. Grice, Rev. Mineral. Geochem. 33 (1996) 41–116.
[26] S.K. Filatov, R.S. Bubnova, Phys. Chem. Glass 41 (2000) 216–224.
[27] F. Liebau, in: Structural Chemistry of Silicates: Structure, Bonding and Classification, Springer-Verlag, Heidelberg, New York, 1985 347p.
[28] N.V. Belov. Ocherki po strukturnoi mineralogii, Moscow: Nedra, 1976, 344p (in Russian).
[29] R.S. Bubnova, S.K. Filatov, in: High-temperature Crystal Chemistry of Borates and Borosilicates, Nauka, St. Petersburg, 2008 760p (in Russian).
[30] Q.-S. Lin, W.-D. Cheng, J.-T. Chen, J.-S. Huang, J. Solid State Chem. 144 (1999) 30–34.
[31] R.S. Bubnova, S.K. Filatov, *Phys. Status Solidi* B 245 (2008) 2469–2476.